LT-LiMn$_{0.5}$Ni$_{0.5}$O$_2$: A Unique Co-Free Cathode for High Energy Li-Ion Cells

Boyu Shi[a], Jihyeon Gim[a], Linze Li[b], Chongmin Wang[b], Anh Vu[a],

Jason R. Croy[a], Michael M. Thackeray[a] and Eungje Lee*[a]

[a]Electrochemical Energy Storage Department, Chemical Sciences and Engineering Division, Argonne National Laboratory, Lemont, IL 60439, United States

[b]Environmental Molecular Sciences Laboratory, Pacific Northwest National Laboratory, Richland, WA 99352, United States

AUTHOR INFORMATION

Corresponding Author

*Eungje Lee (eungje.lee@anl.gov)

ABSTRACT

A new Li-ion battery cathode, 'LT-LiMn$_{0.5}$Ni$_{0.5}$O$_2$', where LT refers to its relatively low synthesis temperature (400 °C), has been identified. Electrochemical data indicate that Li/LT-LiMn$_{0.5}$Ni$_{0.5}$O$_2$ cells operate between 5.0 and 2.5 V with good cycling stability, yielding a cathode capacity of 225 mAh/g. The electrochemical reactions occur in two distinct steps centered at ~3.75 V and ~4.7 V during charge, and at ~4.6 V and ~3.5 V during discharge. High-angle, annular-dark-field (HAADF) scanning-transmission electron microscopy (STEM) provide evidence that LT-LiMn$_{0.5}$Ni$_{0.5}$O$_2$ consists of a unique, partially-disordered LiMn$_{0.5}$Ni$_{0.5}$O$_2$ structure with predominant lithiated-spinel- and layered-like character. Structural analysis of LT-LiMn$_{0.5}$Ni$_{0.5}$O$_2$ with synchrotron X-ray diffraction data shows, surprisingly, that lithiated-spinel and layered models with approximately 16% (~1/6) disorder between the lithium and manganese/nickel ions, yield an identical fit to the data, complicating the determination of the exact nature and level of disorder in each structural model. We believe that this is the first report of a Mn-stabilized, lithium-nickel-oxide spinel-related structure in which the redox reactions occur almost entirely on the nickel ions, with the likelihood that oxygen redox also contributes to some capacity above 4.7 V.

INTRODUCTION

The growing penetration of lithium-ion batteries (LIBs) into the transportation- and stationary-storage markets requires low-cost, high-capacity cathode materials. Recent development of layered $Li(Ni_{1-x-y}Mn_xCo_y)O_2$ cathodes (NMCs) has focused on increasing the nickel content while decreasing the cobalt content to optimize energy and cost. However, the structural and thermal instability of Ni-rich oxides pose concerns about their long-term viability.[1] There is, therefore, a need to develop new cathode materials based on inexpensive, earth-abundant elements, such as Mn and Fe, for further growth and long-term sustainability of the market.[1,2]

$LiMn_2O_4$ (spinel-type) and $LiFePO_4$ (olivine-type) cathodes dominated the early development of commercial LIBs for electric vehicles.[3,4] While NMC cathodes have largely replaced $LiMn_2O_4$ because of their superior electrochemical capacity, $LiFePO_4$ remains attractive as a low-cost alternative.[5] Nevertheless, the family of spinels, $Li[M_2]O_4$, remains an important electrode class because the $[M_2]O_4$ framework provides a unique, interconnected 3-D pathway for rapid lithium-ion diffusion during charge and discharge. Furthermore, selection of the metal cations, M, can be used to tailor the voltage of the spinel cell. From this standpoint, there are still opportunities to exploit spinel oxides for next-generation cathodes. For example, a ~4.7 V $Li/Li_{1-x}Mn_{1.5}Ni_{0.5}O_4$ ($0 \leq x \leq 1$) cell provides an attractive energy density of ~590 Wh/kg relative to a ~4.1 V $Li/Li_{1-x}Mn_2O_4$ cell (~490 Wh/kg).[6] Although further discharge of both these cells can occur at ~3 V to form lithiated-spinels, $Li_2Mn_{1.5}Ni_{0.5}O_4$ and $Li_2Mn_2O_4$, respectively, the reversibility of these reactions is compromised by a crystallographic 'Jahn-Teller' distortion induced by Mn^{3+} ions.[4] In principle, such lithiated-spinel materials, which would allow lithium battery manufacturers to assemble higher capacity cells in a completely discharged state, are typically prepared by impractical soft chemistry methods such as the chemical lithiation of $LiMn_{1.5}Ni_{0.5}O_4$ and $LiMn_2O_4$ with butyllithium.[7,8]

In the early 1990s, Gummow et al. reported a 'low-temperature' form of $LiCoO_2$ (LT-$LiCoO_2$) and Ni-substituted derivatives (LT-$LiCo_{1-x}Ni_xO_2$, $x<0 \leq 0.2$) with a lithiated-spinel-type structure.[9-12] Unfortunately, their low specific capacity (<130 mAh/g), poor cycling stability, and the high cost of cobalt diverted attention from these materials. Nevertheless, motivated by the high intrinsic capacity and the 3-D Li-ion diffusion pathways of fully-lithiated spinel structures, we

recently explored various substituted LT-LiCo$_{1-x}$M$_x$O$_2$ materials, in which Co is partially replaced by an electrochemically-inactive M cation, such as Al^{3+} or Ga^{3+}.[13-15] These studies revealed that Al-substituted LT-LiCo$_{1-x}$Al$_x$O$_2$ (LCAO) cathodes operate with greatly improved cycling stability and 'zero-strain' behavior.[15] Furthermore, the electrochemical signature of LT-LiCo$_{1-x}$Al$_x$O$_2$ differs significantly from lithiated-spinel LT-LiCoO$_2$ and LT-LiCo$_{1-x}$Ni$_x$O$_2$ electrodes, exhibiting apparent single-phase behavior during electrochemical cycling, rather than the typical two-phase behavior expected of an ideally-configured spinel electrode. This difference in behavior was attributed to a small amount of cation disorder between the octahedrally-coordinated Li$^+$, Co^{3+}, and Al^{3+} ions.

Here, we report a new, polymorphic form of LiMn$_{0.5}$Ni$_{0.5}$O$_2$. It has a partially-disordered rock salt structure with predominant lithiated-spinel-like character. This cathode material, denoted LT-LiMn$_{0.5}$Ni$_{0.5}$O$_2$ (or LT-Li$_2$MnNiO$_4$ in lithiated-spinel notation) to differentiate it from the layered, 'high-temperature' HT-LiMn$_{0.5}$Ni$_{0.5}$O$_2$ polymorph, delivers a high specific capacity (225 mAh/g) with good cycling stability over 50 cycles. X-ray diffraction (XRD), high-angle annular dark-field - scanning transmission electron microscopy (HAADF-STEM) and electrochemical methods have been used to probe the structural and electrochemical properties of the electrode. The discovery of LT-LiMn$_{0.5}$Ni$_{0.5}$O$_2$, in which the nickel ions play a significant role in generating stable electrochemical capacity with only a small change to the volume of the cubic unit cell, holds promise for developing a high-capacity, Co-free cathode for an all-solid-state lithium-ion cell.

EXPERIMENTAL

Materials synthesis – A Mn$_{0.5}$Ni$_{0.5}$(OH)$_2$ precursor was synthesized by a co-precipitation method in a continuously-stirred-tank-reactor (CSTR). A stoichiometric amount of Mn$_{0.5}$Ni$_{0.5}$(OH)$_2$ was thoroughly mixed with lithium carbonate (Li$_2$CO$_3$>99%, Sigma-Aldrich) using a mortar and pestle. The mixture was pressed into a pellet and calcined at a 'low-temperature' (LT) of 400 °C for 72 h in air. The heating rate was 2 °C/min while cooling was uncontrolled. The calcined pellet was ground to obtain a homogeneous fine powder.

Materials characterization – The quality and structure of the LT-LiMn$_{0.5}$Ni$_{0.5}$O$_2$ product was first characterized by X-ray diffraction (XRD) using a laboratory Rigaku MiniFlex 600 diffractometer with Cu Kα radiation (1.5406 Å). High resolution synchrotron XRD data were subsequently obtained using the synchrotron 11-ID-C beamline (calibrated wavelength: 0.1173 Å) at the Advanced Photon Source (APS), Argonne National Laboratory. The data were collected in transmission mode using a spinning Kapton capillary tube. Rietveld refinement analyses of the LT-LiMn$_{0.5}$Ni$_{0.5}$O$_2$ sample were conducted with the TOPAS software package.

The particle morphology was studied using scanning electron microscopy (SEM) (JCM-6000 PLUS Neoscope microscope). Specimens for high-angle annular dark-field (HAADF) scanning transmission electron microscopy (STEM) characterization were prepared with a routine focused-ion-beam (FIB) lifting-out procedure using a Thermo Scientific Helios DualBeam microscope working at 2-30 keV. HAADF STEM imaging was performed on an aberration-corrected JEOL GrandARM-300F microscope with an operation voltage of 300 kV. The convergence semi-angle was 22.4 mrad; signals with semi-angles spanning from 60 to 409 mrad were collected for HAADF STEM imaging.

Mn K-edge and Ni K-edge XAS data were collected at the 12-BM beamline of the APS. The standard samples for Mn^{n+} (n = 4) and Ni^{n+} (n = 2 and 3) were prepared as 7mm diameter pellets with boron nitride as a dispersing agent. In addition, a Ni$^{3.7+}$ standard sample was produced electrochemically by charging a Li/LiNiO$_2$ cell to 4.4 V to the cathode composition Li$_{0.3}$NiO$_2$. All spectra were collected in transmission mode; the data were reduced using ATHENA in the Demeter software package. The standard Mn K-edge (6539 eV) and Ni K-edge (8333 eV) energy was calibrated and aligned using the first inflection point of the edge region of a metallic Mn and Ni foil collected simultaneously with each measurement. For each spectrum, the built-in AUTOBK algorithm was used to normalize the absorption coefficient, $\mu(k)$, and separate the $\chi(k)$ functions from the isolated atom absorption background. The extracted EXAFS signal, $\chi(k)$, was weighted by k^2; fourier transform (FT) was then applied in k-ranges of 3.0–9.749 Å^{-1} for Mn and 2.7-11.8 Å^{-1} for Ni, respectively, using the Hanning window function to obtain the magnitude plots of the EXAFS spectra in R-space (Å). The FT peaks were not phase-corrected, and thus the actual bond lengths are approximately 0.2–0.4 Å longer.

Electrochemical testing and ex situ electrodes analysis – LT-LiMn$_{0.5}$Ni$_{0.5}$O$_2$ cathode laminates were prepared by coating a cathode slurry on aluminum foil. The composition of the slurry was 84 wt% active material: 8 wt% super P carbon: 8 wt % polyvinylidene difluoride (Solvay) binder homogeneously dispersed in an N-methyl-2-pyrrolidone (NMP) solvent. Electrochemical tests were conducted using 2032-type coin cells that were assembled in an Ar-filled glovebox. A lithium metal chip was used as the anode. The electrolyte was made of 1.2 M lithium hexafluorophosphate (LiPF$_6$) dissolved in a 3:7 mixture solvent of ethylene carbonate (EC) and ethyl methyl carbonate (EMC). The coin cells were placed in a climate chamber, which was maintained at 30 ^{o}C, and tested using a MACCOR battery cycler. For *ex situ* XRD and XAS tests, the charged/discharged electrode samples were collected from the disassembled coin cells in an Ar-filled glove box. The harvested electrodes were sealed with Kapton film to prevent air exposure.

RESULTS AND DISCUSSIONS

LT-LiMn$_{0.5}$Ni$_{0.5}$O$_2$ was synthesized by the solid-state reaction of Li$_2$CO$_3$ and Mn$_{0.5}$Ni$_{0.5}$(OH)$_2$ precursors in air at 400 °C, the XRD pattern of which could be indexed to a cubic unit cell with lattice parameter, a = 8.217 Å (Fig. 1 and 2). In contrast, the layered polymorph, HT-LiMn$_{0.5}$Ni$_{0.5}$O$_2$ prepared at 900 °C in oxygen, has a trigonal unit cell with a c/a ratio = 4.95 in which the Li$^+$ and Ni^{2+} ions are disordered between the layers by ~11%.[16] This difference in crystallographic symmetry is evident from the distinct splitting of the (440) peak of cubic LT-LiMn$_{0.5}$Ni$_{0.5}$O$_2$ at approximately 65 °2θ (i.e., ~4.62 °2θ with λ = 0.1173 Å radiation) into the (110) and (108) peaks of trigonal HT-LiMn$_{0.5}$Ni$_{0.5}$O$_2$ (Fig. 1).
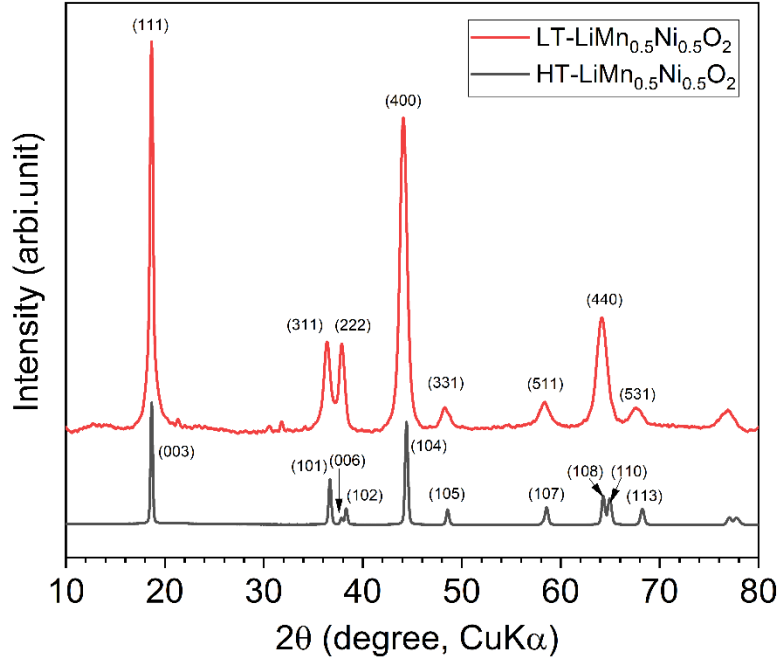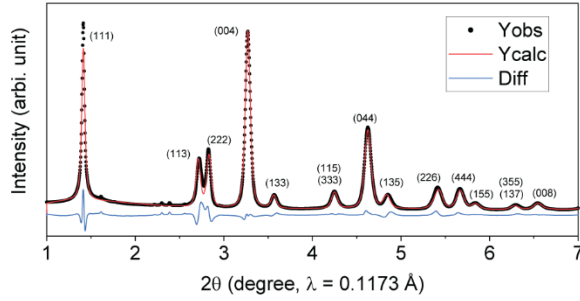
Figure 1. Comparison of XRD patterns for LT-LiMn$_{0.5}$Ni$_{0.5}$O$_2$ and HT-LiMn$_{0.5}$Ni$_{0.5}$O$_2$ samples. The HT-sample, which has a layered structure, was synthesized in air at 850 °C for 15h.

Given the apparent single-phase character of the synchrotron XRD pattern of LT-LiMn$_{0.5}$Ni$_{0.5}$O$_2$, Rietveld refinements were undertaken to determine the structure-type and the extent of disorder, if any, between the lithium, manganese, and nickel ions on the octahedral sites of the cubic-close-packed oxygen array (Fig. 2). When constraining the Mn:Ni ratio of 1:1, a good fit to the XRD data was achieved with a cubic lithiated-spinel model, Li$_2^{(16c)}$M$_2^{(16d)}$O$_4$ (M=Mn, Ni; space group Fd-3m), in which 16.6% (~1/6) of the Li ions on the 16c sites were exchanged with Mn/Ni ions on the 16d sites, thereby yielding a disordered rock salt configuration with strong lithiated-spinel character, (Li$_{0.83}$M$_{0.17}$)$_2^{(16c)}$[Li$_{0.17}$M$_{0.83}$]$_2^{(16d)}$O$_4$ (Fig. 2a). This level of Li/M site-exchange is significantly higher than it is in the Co-based lithiated-spinel material, LT-LiCo$_{0.85}$Al$_{0.15}$O$_2$ in which there is only ~2% of site-exchange between the lithium and cobalt/aluminum ions.[15] The weighted R$_{wp}$ factor for this refinement was 8.56%.

Figure 2. Rietveld refinement of LT-LiMn$_{0.5}$Ni$_{0.5}$O$_2$ with (a) partially-disordered lithiated-spinel and (b) partially-disordered layered models.

(a) Lithiated spinel structure model

Phase: Lithiated-spinel Li$_2$MnNiO$_4$ (S.G. Fd-3m)
a = 8.217 Å; R_{wp} = 8.56 %

Atom	Site	x	y	z	Occ	B$_{eq}$
Li1	16c	0	0	0	0.834	1
Li2	16d	0.5	0.5	0.5	0.166	1
Mn1	16c	0	0	0	0.083	1
Mn2	16d	0.5	0.5	0.5	0.417	1
Ni1	16c	0	0	0	0.083	1
Ni2	16d	0.5	0.5	0.5	0.417	1
O	32e	0.258	0.258	0.258	1	1.691

(b) Cubic layered structure model
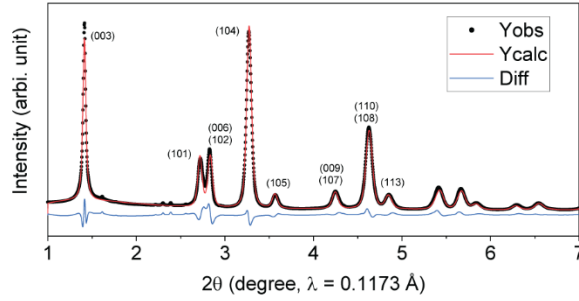
Phase: Layered Li$_2$MnNiO$_4$ (S.G. R-3m)
a = 2.902 Å, c = 14.277 Å (c/a = 4.92); R_{wp} = 8.80 %

Atom	Site	x	y	z	Occ	B$_{eq}$
Li1	3a	0	0	0	0.838	1
Li2	3b	0	0	0.5	0.162	1
Mn1	3a	0	0	0	0.081	1
Mn2	3b	0	0	0.5	0.419	1
Ni1	3a	0	0	0	0.081	1
Ni2	3b	0	0	0.5	0.419	1
O	6c	0	0	0.242	1	1.605

Remarkably, an essentially identical fit to the XRD data of LT-LiMn$_{0.5}$Ni$_{0.5}$O$_2$ was obtained with a disordered, layered model (Li$_{0.838}$M$_{0.162}$)$^{(3a)}$[Li$_{0.162}$M$_{0.838}$]$^{(3b)}$O$_2$ (space group R-3m) in which 16.2% (~1/6) of the M ions on the 3b sites are located in the 3a sites of the Li-rich layers of an essentially cubic-close-packed structure, and vice versa (Fig. 2b). In this case, the weighted R$_{wp}$ factor was 8.80%. Refinement of this model with R-3m symmetry yielded a c/a ratio = 4.92 which is close to the theoretical ratio for a cubic unit cell (c/a = 4.90) and significantly less than that of HT-LiMn$_{0.5}$Ni$_{0.5}$O$_2$ with ~11% disorder (c/a = 4.95).[16] Note that a perfectly ordered cubic, lithiated-spinel structure, such as Li$_2$[Co$_2$]O$_4$ (LT-LiCoO$_2$) and its layered counterpart, LiCoO$_2$, would have an identical atomic vector space and hence an identical X-ray diffraction pattern, but only if the layered LiCoO$_2$ structure is ideally cubic-close-packed (c/a=4.90) which, in practice, it is not (c/a=4.99).[17] Note also that the average degree of disorder in such LT-LiMn$_{0.5}$Ni$_{0.5}$O$_2$ model structures, 16-17%, lies between that observed in layered HT-LiMn$_{0.5}$Ni$_{0.5}$O$_2$ (~11%)[16] and the cation distribution in an ideal, ordered lithiated-spinel structure, such as Li$_2$$^{(16c)}$[Mn$_2$]$^{(16d)}O_4$ (or hypothetical LT-Li$_2$$^{(16c)}$[MnNi]$^{(16d)}O_4$), in which 25% of the transition metal ions reside in 16d sites in the lithium-rich layers, and 25% of the lithium ions reside in 16c sites in the transition-metal-rich layers.

Because the X-ray diffraction pattern of the LT-LiMn$_{0.5}$Ni$_{0.5}$O$_2$ electrode reflects an averaged atomic arrangement, a Rietveld refinement of a cubic LiMn$_{0.5}$Ni$_{0.5}$O$_2$ model structure composed of regions with fully-ordered lithiated-spinel, Li$_2$[MnNi]O$_4$, and partially-disordered, layered HT-LiMn$_{0.5}$Ni$_{0.5}$O$_2$ arrangements could, in principle, also yield a structure with an apparent 16-17% (~1/6) disorder of the lithium and transition metal ions. This possibility complicates the interpretation of the structural refinement. However, given the 11% disorder between the lithium and nickel ions in layered HT-LiMn$_{0.5}$Ni$_{0.5}$O$_2$,[16] we suspect, likewise, that the disorder in the LT-LiMn$_{0.5}$Ni$_{0.5}$O$_2$ structure occurs between the lithium and nickel ions such that the nickel ions reside only in the lithium-rich layer, thereby bringing some equivalence to the X-ray diffraction patterns of the partially-disordered lithiated-spinel and layered models. Furthermore, from a crystallographic standpoint, the degree of disorder (~1/6), suggests that there may likely be 'order within the disorder' and, therefore, that the lithiated-spinel and layered structures would have lower symmetry than their parent space groups, Fd-3m and R-3m, respectively. Such ordering, rather than a random disorder of the lithium and transition-metal ions in alternate layers, would enhance 2-D diffusion within the layered arrangements and 3-D diffusion within the lithiated-spinel arrangements of the structure.

A scanning electron microscopy image of LT-LiMn$_{0.5}$Ni$_{0.5}$O$_2$ shows a spherically-shaped, secondary particle morphology with a particle-size distribution from 5 to 15 μm in diameter (Fig. 3a). To observe the internal atomic structure of the secondary particle, the LT-LiMn$_{0.5}$Ni$_{0.5}$O$_2$ sample was cross-sectioned by focused ion-beam milling. The HAADF-STEM image in Fig. 3b shows atomic arrangements consistent with the [110] zone axis of a lithiated-spinel structure. In the magnified image of Fig. 3b, the atomic contrast in the high-resolution image perfectly matches the [110] directional view of the lithiated-spinel model, in which the magenta and yellow spots represent M-only and mixed M/Li columns, respectively. The atomic contrast in the LT-LiMn$_{0.5}$Ni$_{0.5}$O$_2$ images is significantly less pronounced than it is in images of the well-ordered lithiated-spinel LT-LiCoO$_2$ structure.[13] Inspection of multiple images revealed localized domains that could be assigned predominantly to lithiated-spinel and layered atomic arrangements, but also to some more highly disordered rock salt regions (Figs. 3c and d).
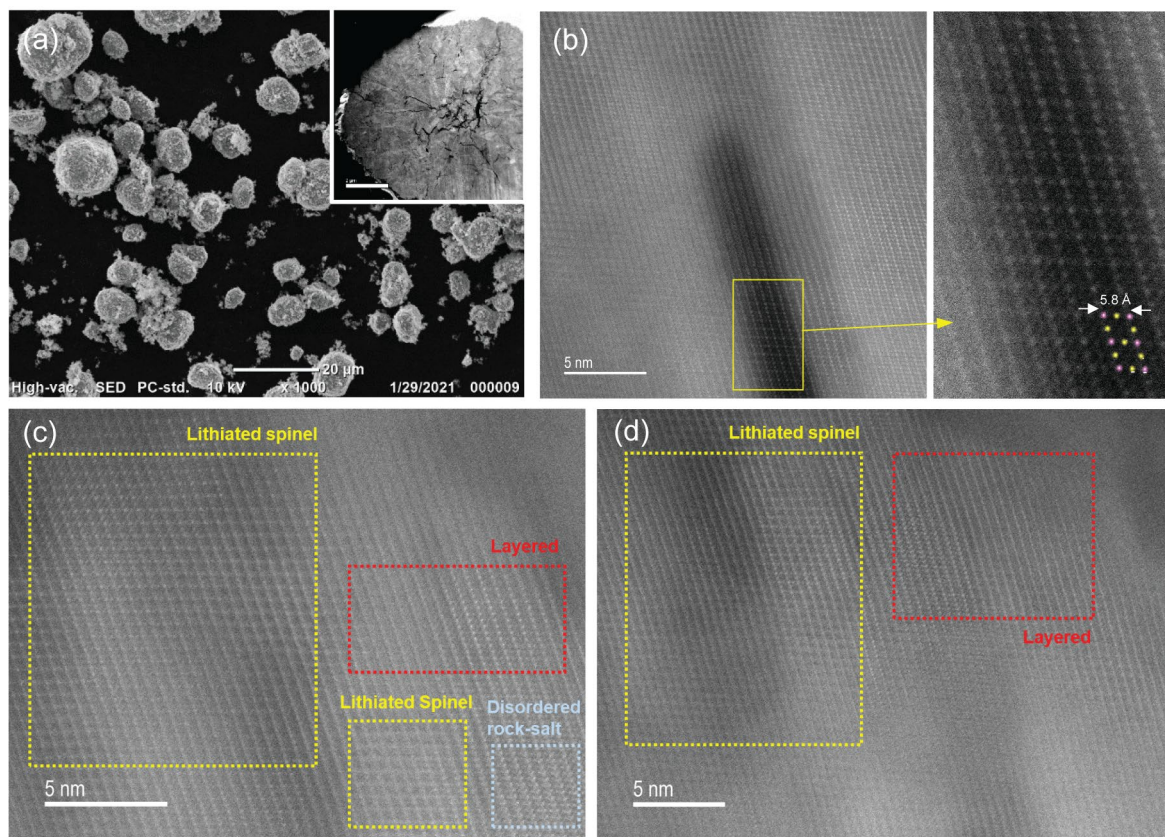
Figure 3. (a) SEM and (b-d) HAADF-STEM images of LT-LiMn$_{0.5}$Ni$_{0.5}$O$_2$.

Figure 4a shows the electrochemical signature of a Li/LT-LiMn$_{0.5}$Ni$_{0.5}$O$_2$ cell when cycled between 5.0 and 2.5 V. After one formation cycle, the cell shows stable cycling behavior while delivering a cathode discharge capacity of 225 mAh/g. The charge profile is characterized by two dominant voltage 'plateaus', centered at ~3.75 V and ~4.7 V during charge, and at ~4.6 V and ~3.5 V during discharge. The dQ/dV plot in Fig. 4b reveals that the 'low-voltage' (LV) plateau is associated with two processes at 3.5 and 3.6 V that can be attributed to lithium extraction from octahedral sites and nickel oxidation in the delithiated spinel and layered regions of the electrode structure, respectively. The high-voltage (HV) plateau is associated with three distinct processes, the first of which at ~4.5 V is attributed to lithium extraction from tetrahedral sites and nickel oxidation in the spinel and layered domains while the two, relatively weak, but pronounced, reactions seen in the dQ/dV plot between 4.6 and 4.7 V are attributed, tentatively, to further nickel oxidation and participation of oxygen ions in the electrochemical reaction.
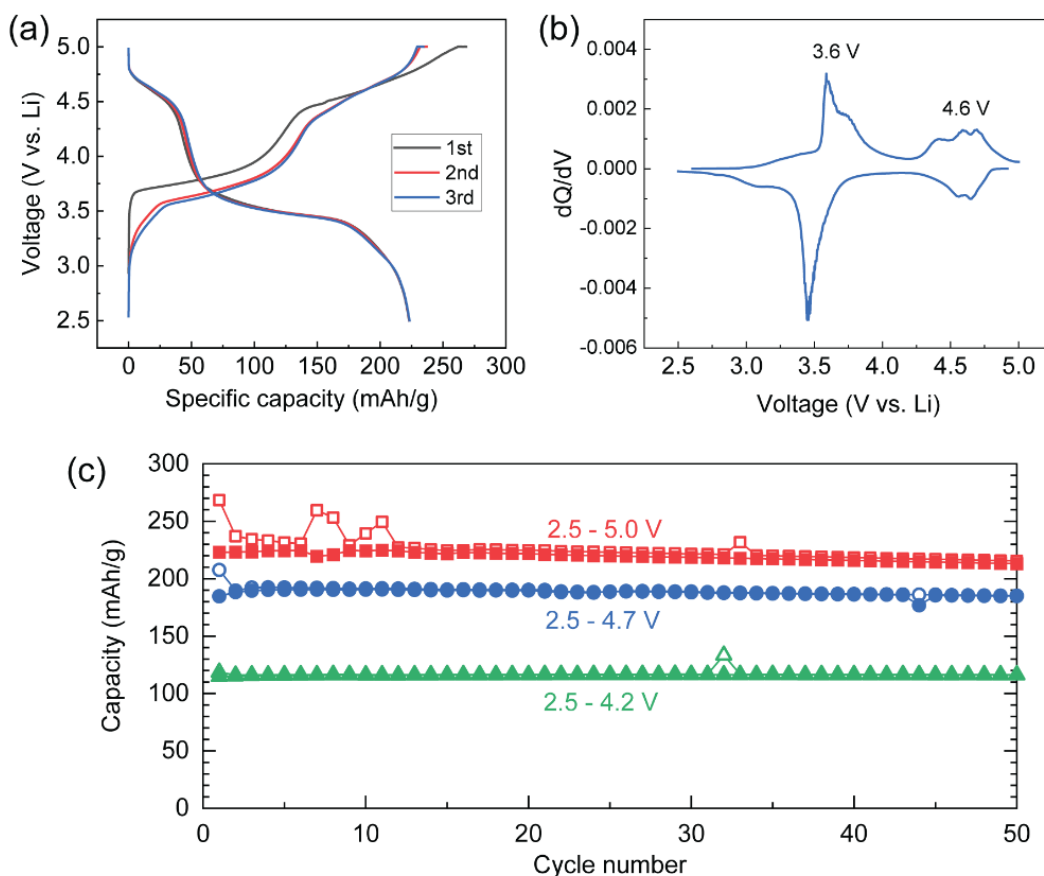
Figure 4. (a) Voltage profiles of Li/LT-LiMn$_{0.5}$Ni$_{0.5}$O$_2$ cells (i = 15 mA/g), (b) corresponding differential capacity (dQ/dV) plot (2nd cycle), and (c) cycling stability (open = charge, solid = discharge).

Preliminary ex-situ X-ray absorption spectroscopy (XAS) data confirm that the redox reactions occur predominantly on the nickel ions, and that the manganese and nickel ions in pristine and cycled LT-LiMn$_{0.5}$Ni$_{0.5}$O$_2$ electrodes are tetravalent and divalent, respectively, as they are in HT-LiMn$_{0.5}$Ni$_{0.5}$O$_2$ (Fig. 5). All these reactions are apparently reversible. A weak peak at 3 V in the dQ/dV plot of the discharge reaction is consistent with a minor Mn$^{4+/3+}$ redox reaction in the spinel-like domains (Fig. 4b).
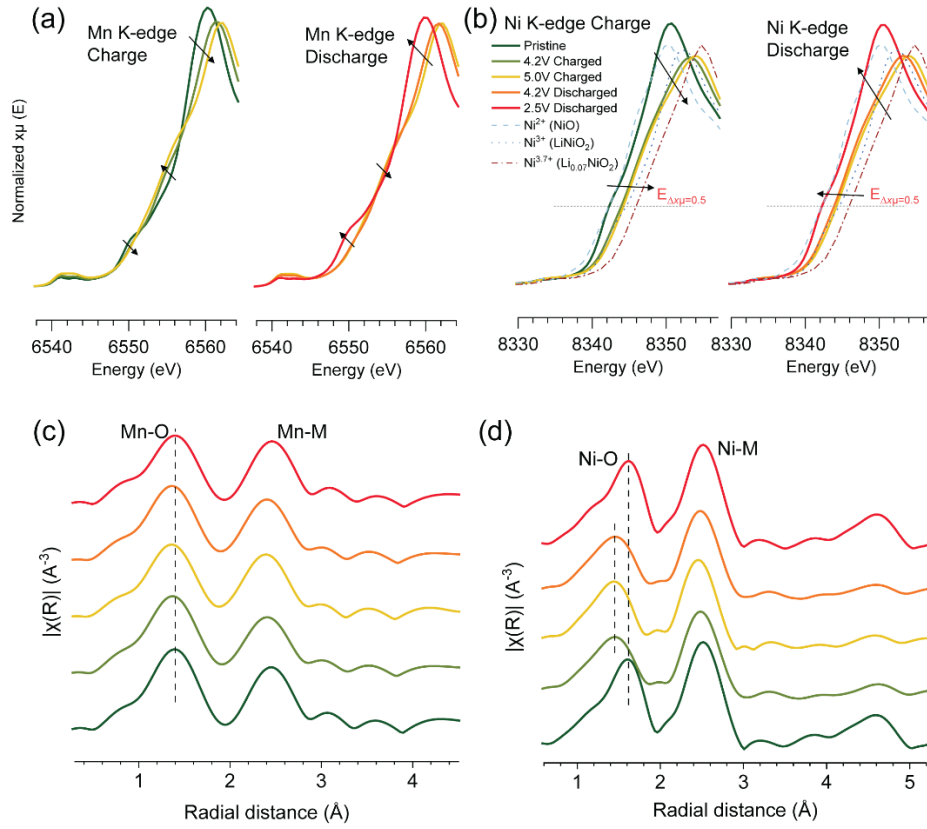
Figure 5. *Ex situ* Mn K-edge and Ni K-edge XAS analysis of LT-LiMn$_{0.5}$Ni$_{0.5}$O$_2$. Normalized (a) Mn and (b) Ni K-edge XANES spectra. K^2-weighted Fourier transform (FT) magnitudes of (c) Mn and (d) Ni K-edge EXAFS spectra.

The LV plateau on the initial charge corresponds to the extraction of 0.9 Li from the LT-LiMn$_{0.5}$Ni$_{0.5}$O$_2$ electrode and a specific capacity of ~130 mAh/g, while the HV plateau accounts for a further extraction of ~0.8 Li and a specific capacity of ~110 mAh/g (Fig. 4a); these two plateaus are attributed to lithium extraction from octahedral and tetrahedral sites, respectively. On the subsequent discharge, the HV capacity decreases to ~50 mAh/g (~0.35 Li intercalation) while the LV capacity increases to ~170 mAh/g (~1.2 Li intercalation). We tentatively ascribe this asymmetry in electrochemical behavior (polarization) to subtle structural changes that ease the extraction of lithium during the charging process, and to reverse effects during discharge. Despite these polarizing effects, our preliminary results demonstrate that Li/LT-LiMn$_{0.5}$Ni$_{0.5}$O$_2$ cells cycle with good electrochemical stability between 5.0 and 2.5 V, yielding ~96% capacity retention over 50 cycles (Fig. 4c), during which the electrochemical profile changes slightly. Furthermore, XRD patterns of cycled electrodes show no evidence of any significant structural degradation (Fig. 6).
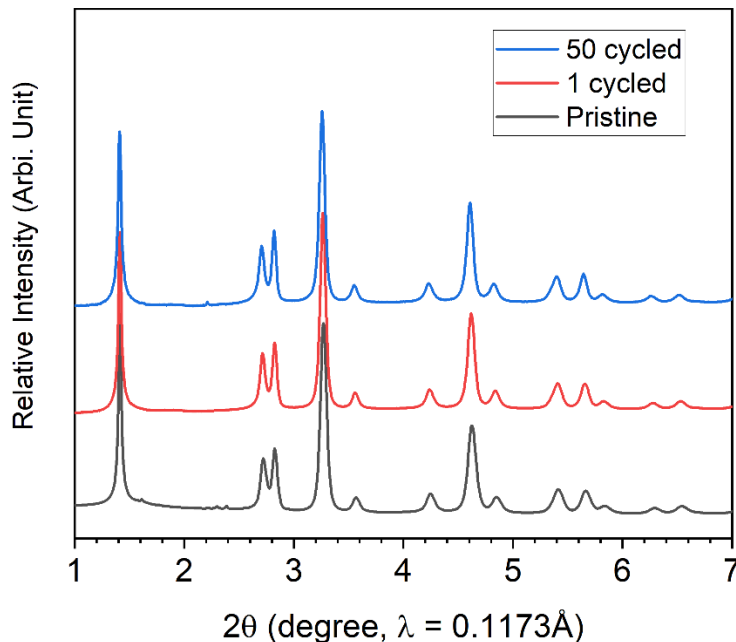
Figure 6. *Ex situ* synchrotron XRD patterns of LT-LiMn$_{0.5}$Ni$_{0.5}$O$_2$ electrodes in their discharged state. Bottom to top: pristine electrode; after 1 cycle, and after 50 cycles ($v = 2.5 – 5.0$ V; $i = 15$ mAh/g).

Viewed overall, the XRD data, electrochemical profile, dQ/dV plot and HAADF-STEM images support a complex structural model for LT-LiMn$_{0.5}$Ni$_{0.5}$O$_2$ with predominant, disordered lithiated-spinel character, which coexists with disordered layered-like domains, while the high, accessible capacity (225 mAh/g) likely reflects cation ordering, rather than random disorder.

Synchrotron XRD patterns of LT-LiMn$_{0.5}$Ni$_{0.5}$O$_2$ electrodes, collected *ex situ* at different states-of-charge during the initial charge, reveal that the (111) peak shifts reversibly during cycling (Fig. 7, left and middle panels) and that the close-packed oxygen array of the structure maintains its cubic symmetry. During charge and discharge, the unit cell volume contracts and expands by only 2.7%, which is significantly less than the volume change observed in the spinel electrodes, Li$_x$Mn$_2$O$_4$ (16%) and Li$_x$Mn$_{1.5}$Ni$_{0.5}$O$_4$ (12%), over the wide compositional range $0 \leq x \leq 2$.[18-19] Note that the (113) and (222) peaks show reversible changes, not only in their 2θ positions but also in their peak intensities (Fig. 7, right panel), confirming reversible atomic rearrangements within the structure. A Rietveld refinement of a delithiated LT-Li$_{1-x}$Mn$_{0.5}$Ni$_{0.5}$O$_2$ electrode after charging to 4.2 V is consistent with a spinel-like structure in which Li occupies tetrahedral sites (Fig. 8).
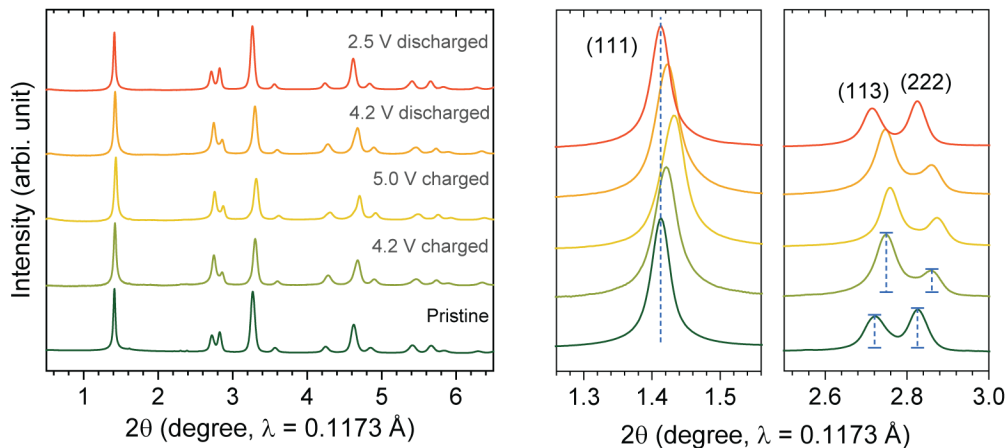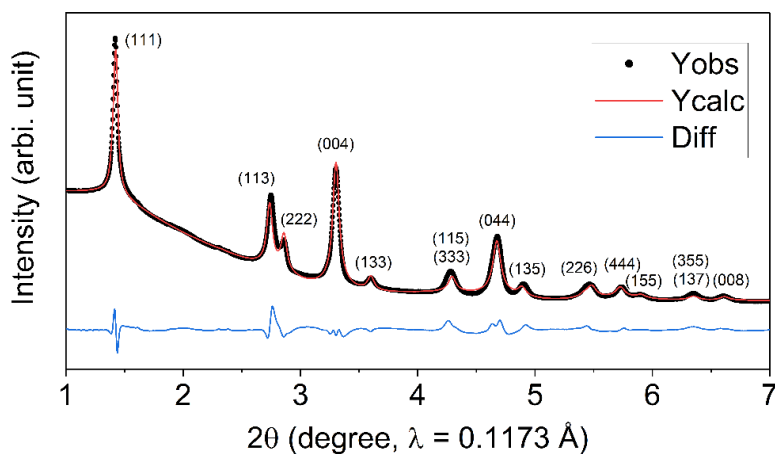
Figure 7. Synchrotron XRD patterns of LT-LiMn$_{0.5}$Ni$_{0.5}$O$_2$ electrodes at various states of charge (1st cycle).

Atom	Site	x	y	z	Occ	B$_{eq}$
Li1	8a	0.125	0.125	0.125	0.81	1
Li2	16d	0.5	0.5	0.5	0.166	1
Mn1	16c	0	0	0	0.083	1
Mn2	16d	0.5	0.5	0.5	0.417	1
Ni1	16c	0	0	0	0.083	1
Ni2	16d	0.5	0.5	0.5	0.417	1
O	32e	0.2537	0.2537	0.2537	1	2.546

Figure 8. *Ex situ* synchrotron XRD pattern and Rietveld refinement results of a delithiated LT-Li$_{1-x}$Mn$_{0.5}$Ni$_{0.5}$O$_2$ electrode using a spinel model (LT-Li$_{2-y}$MnNiO$_4$, y ~1.0) collected at 4.2 V. Space group Fd-3m; a = 8.1307 Å; R_{wp} = 3.73%.

When lithium- and manganese-rich electrodes, such as layered $Li_{1.13}Mn_{0.57}Ni_{0.30}O_2$ (alternatively, $0.3Li_2MnO_3 \bullet 0.7LiMn_{0.5}Ni_{0.5}O_2$)[20] and spinel $Li_4Mn_5O_{12}$[21], are charged repeatedly to potentials above 4.6 V, lithium is extracted with concomitant oxygen loss (net loss = Li_2O). In the former case, electrochemical cycling is accompanied by voltage fade and the gradual migration of cations from one layer to the next,[20] while lithium and oxygen loss from $Li_4Mn_5O_{12}$ ($2Li_2O \bullet 5MnO_2$) results in an electrochemical profile that increasingly resembles that of a Li-rich $Li_{1+x}Mn_{2-x}O_4$ spinel electrode ($0<x<0.33$) with a composition between $LiMn_2O_4$ and $Li_4Mn_5O_{12}$.[21] In contrast, LT-$LiMn_{0.5}Ni_{0.5}O_2$, which is not lithium-rich, has an electrochemical profile that is notably more tolerant and stable to repeated charging to 5 V (Fig. 3a) illustrating the superior robustness of the partially-disordered lithiated-spinel electrode. It should be noted that LT-$LiMn_{0.5}Ni_{0.5}O_2$ can also be regarded, overall, as having a partially-disordered rock salt structure, which delivers most of its capacity in two discrete steps centered at ~4.6 V and ~3.5 V during discharge, unlike the Li-rich, disordered rock salt electrode structures described by Meng et al.[22] and partially-disordered lithium-metal oxyfluoride rock salt electrodes reported by Ceder et al.[23] that discharge their capacity with a continuous drop in voltage between 4.7 and 1.5 V.

Table 1 compares the Li intercalation potentials of various spinel cathodes. The data emphasize the versatility of lithium-manganese-oxide and nickel-substituted spinel electrode structures and compositions in tailoring the voltage of a lithium cell. While a $Li_xMn_2O_4$ spinel electrode ($0 \leq x \leq 2$) delivers its capacity over two distinct plateaus at 3.0 and 4.1 V involving manganese redox reactions, the nickel-substituted $Li_xMn_{1.5}Ni_{0.5}O_4$ spinel electrode involves both manganese and nickel redox reactions at 3.0 and 4.7 V, respectively. On the other hand, the LT-$LiMn_{0.5}Ni_{0.5}O_2$ lithiated-spinel configuration identified in this preliminary study operates predominantly by redox reactions at 3.6 and 4.6 V on the nickel ions and, likely, by some oxygen redox above 4.7 V. The electrochemical reaction also includes a minor amount of manganese redox at 3 V. Of particular significance is that LT-$LiMn_{0.5}Ni_{0.5}O_2$ offers the highest average voltage of these cobalt-free spinel systems.

Table 1. Reaction potentials (vs. Li^0) and corresponding redox couples in spinel cathodes.

Li site	$Li_xMn_2O_4$[18]	$Li_xMn_{1.5}Ni_{0.5}O_4$[19]	LT-$Li_xMn_{0.5}Ni_{0.5}O_2$* [This work]
Tetrahedral Li ($0 \leq x \leq 1$)	4.1 V Mn^{3+}/Mn^{4+}	4.7 V $Ni^{2+}/Ni^{3+}/Ni^{4+}$	4.5-4.7 V Ni^{3+}/Ni^{4+}; O redox?
Octahedral Li ($1 \leq x \leq 2$)	3.0 V Mn^{3+}/Mn^{4+}	3.0 V Mn^{3+}/Mn^{4+}	3.6 V Ni^{2+}/Ni^{3+} 3.0 V Mn^{4+}/Mn^{3+} (minor)

*Spinel component only

CONCLUSIONS

The discovery of LT-$LiMn_{0.5}Ni_{0.5}O_2$, not only expands the compositional space of the known spinel family; it also holds promise for designing a solid state $Li_4Ti_5O_{12}$/LT-$LiMn_{0.5}Ni_{0.5}O_2$ 'spinel-lithiated spinel' cell that would operate between 3.0 and 2.0 V. The concept of exploiting partially-disordered lithiated-spinel electrodes certainly warrants further study and understanding, both experimental and theoretical, as does the unique structural relationship that appears to exist between lithiated-spinel and layered cation arrangements in LT-$LiMn_{0.5}Ni_{0.5}O_2$.

REFERENCES

(1) Li, W.; Erickson, E. M.; Manthiram, A. High-Nickel Layered Oxide Cathodes for Lithium-Based Automotive Batteries. *Nat. Energy* **2020,** *5*, 26-34.

(2) Croy, J. R.; Gutierrez, A.; He, M.; Yonemoto, B. T.; Lee, E.; Thackeray, M. M. Development of Manganese-Rich Cathodes as Alternatives to Nickel-Rich Chemistries. *J. Power Sources* **2019,** *434*, 226706.

(3) Manthiram, A. A Reflection on Lithium-Ion Battery Cathode Chemistry. *Nat. Commun.* **2020,** *11*, 1550.

(4) Thackeray, M. M. Exploiting the Spinel Structure for Li-ion Battery Applications: A Tribute to John B. Goodenough. *Advan. Energy Mater.* **2020**, 2001117.

(5) Yang, X.-G.; Liu, T.; Wang, C.-Y. Thermally Modulated Lithium Iron Phosphate Batteries for Mass-Market Electric Vehicles. *Nat. Energy* **2021**, *6*, 176-185.

(6) Huang, Y.; Dong, Y.; Li, S.; Lee, J.; Wang, C.; Zhu, Z.; Xue, W.; Li, Y.; Li, J. Lithium Manganese Spinel Cathodes for Lithium-Ion Batteries. *Advan. Energy Mater.* **2020,** *11*, 2000997.

(7) David, W. I. F.; Goodenough, J. B.; Thackeray, M. M.; Thomas, M. G. S. R. The crystal structure of Li_2MnO_2. *Rev. Chim. Miner.* **1983,** *20*, 636-642.

(8) Dose, W. M.; Blauwkamp, J.; Piernas-Muñoz, M. J.; Bloom, I.; Rui, X.; Klie, R. F.; Senguttuvan, P.; Johnson, C. S. Liquid Ammonia Chemical Lithiation: An Approach for High-Energy and High-Voltage Si–Graphite|$Li_{1+x}Ni_{0.5}Mn_{1.5}O_4$ Li-Ion Batteries. *ACS Appl. Energy Mater.* **2019,** *2*, 5019-5028.

(9) Gummow, R. J.; Thackeray, M. M.; David, W. I. F.; Hull, S. Structure and Electrochemistry of Lithium Cobalt Oxide Synthesized at 400^oC. *Mater. Res. Bull.* **1992,** *27* (3), 327-337.

(10) Gummow, R. J.; Liles, D. C.; Thackeray, M. M.; David, W. I. F. A Reinvestigation of the Structures of Lithium-Cobalt-Oxides with Neutron-Diffraction Data. *Mater. Res. Bull.* **1993,** *28*, 1177-1184.

(11) Gummow, R. J.; Thackeray, M. M. Lithium-Cobalt-Nickel-Oxide Cathode Materials Prepared at 400^oC for Rechargeable Lithium Batteries. *Solid State Ionics* **1992,** *53*, 681-687.

(12) Gummow, R. J.; Thackeray, M. M. Characterization of LT-$Li_xCo_{1-y}Ni_yO_2$ Electrodes for Rechargeable Lithium Cells. *J. Electrochem. Soc.* **1993,** *140*, 3365-3368.

(13) Lee, E.; Blauwkamp, J.; Castro, F. C.; Wu, J.; Dravid, V. P.; Yan, P.; Wang, C.; Kim, S.; Wolverton, C.; Benedek, R.; Dogan, F.; Park, J. S.; Croy, J. R.; Thackeray, M. M. Exploring Lithium-Cobalt-Nickel Oxide Spinel Electrodes for ≥3.5 V Li-Ion Cells. *ACS Appl. Mater. Inter.* **2016,** *8*, 27720-27729.

(14) Kim, S.; Hegde, V. I.; Yao, Z.; Lu, Z.; Amsler, M.; He, J.; Hao, S.; Croy, J. R.; Lee, E.; Thackeray, M. M.; Wolverton, C. First-Principles Study of Lithium Cobalt Spinel Oxides: Correlating Structure and Electrochemistry. *ACS Appl. Mater. Inter.* **2018,** *10*, 13479-13490.

(15) Lee, E.; Kwon, B. J.; Dogan, F.; Ren, Y.; Croy, J. R.; Thackeray, M. M. Lithiated Spinel $LiCo_{1-x}Al_xO_2$ as a Stable Zero-Strain Cathode. *ACS Appl. Energy Mater.* **2019,** *2*, 6170-6175.

(16) Meng, Y. S.; Ceder, G.; Grey, C. P.; Yoon, W.-S.; Jiang, M.; Bréger, J.; Shao-Horn, Y. Cation Ordering in Layered O3 $Li[Ni_xLi_{1/3-2x/3}Mn_{2/3-x/3}]O_2$ ($0 \leq x \leq 1/2$) Compounds. *Chem. Mater.* **2005,** *17*, 2386-2394.

(17) Rossen, E; Reimers, J. N.; Dahn, J. R. Synthesis and Electrochemistry of Spinel LT-$LiCoO_2$. *Solid State Ionics* **1993,** *62*, 53-60.

(18) Thackeray, M. M. Spinel Electrodes for Lithium Batteries. *J. Am. Ceram. Soc.* **1999**, *82*, 3347-3354.

(19) Lee, E.-S.; Nam, K.-W.; Hu, E.; Manthiram, A. Influence of Cation Ordering and Lattice Distortion on the Charge–Discharge Behavior of $LiMn_{1.5}Ni_{0.5}O_4$ Spinel between 5.0 and 2.0 V. *Chem. Mater.* **2012**, *24*, 3610-3620.

(20) Johnson, C. S.; Kim, J-S.; Lefief, C.; Li, N.; Vaughey, J. T. and Thackeray, M. M. The Significance of the Li_2MnO_3 Component in 'Composite' x $Li_2MnO_3 \bullet (1-x)LiMn_{0.5}Ni_{0.5}O_2$ Electrodes, Electrochem. Commun. **2004**, *6*, 1085-1091.

(21) Liu, Y.; Liu, G.; Xu, H.; Zheng, Y.; Huang, Y.; Li, S.; Li, J. Low-Temperature Synthesized $Li_4Mn_5O_{12}$-like Cathode with Hybrid Cation- and Anion-Redox Capacities. *Chem. Commun.* **2019,** *55*, 8118-8121.

(22) Chung, H.; Lebens-Higgins, Z.; Sayahpour, B.; Mejia, C.; Grenier, A.; Kamm, G. E.; Li, Y.; Huang, R.; Piper, L. F. J.; Chapman, K. W.; Doux, J.-M. and Meng, Y. S. Experimental considerations to study Li-excess disordered rock salt cathode materials. *J. Mater. Chem. A*, **2021**, *9*, 1720-1732.

(23) Ji, H.; Wu, J.; Cai, Z.; Liu, J.; Kwon, D-H.; Kim, H.; Urban, A.; Papp, J. K.; Foley, E.; Tian, Y.; Balasubramanian, M.; Kim, H.; Clément, R. J.; McCloskey, B. D.; Yang, W. and Ceder, G.

Ultrahigh power and energy density in partially ordered lithium-ion cathode materials. *Nature Energy* **2020**, *5*, 213–221.